

Few-Body Analog Quantum Simulation with Rydberg-Dressed Atoms in Optical Lattices

Daniel Malz^{1,2,*} and J. Ignacio Cirac^{1,2}

¹Max Planck Institute for Quantum Optics, Hans-Kopfermann-Straße 1, Garching D-85748, Germany

²Munich Center for Quantum Science and Technology, Schellingstraße 4, München D-80799, Germany

 (Received 12 December 2022; revised 7 February 2023; accepted 22 February 2023; published 3 April 2023)

Most experiments with ultracold atoms in optical lattices have contact interactions and therefore operate at high densities of around one atom per site to observe the effect of strong interactions. Strong ranged interactions can be generated via Rydberg dressing, which opens up the path to exploring the physics of few interacting particles. Rather than the unit cells of a crystal, the sites of the optical lattice can now be interpreted as discretized space. This allows the study of completely new types of problems in a familiar architecture. We investigate the possibility of realizing problems akin to those found in quantum chemistry, although with a different scaling law in the interactions. Through numerical simulation, we show that simple pseudoatoms and pseudomolecules could be prepared with high fidelity in state-of-the-art experiments.

DOI: [10.1103/PRXQuantum.4.020301](https://doi.org/10.1103/PRXQuantum.4.020301)

I. INTRODUCTION

Analog quantum simulation with ultracold atoms trapped in optical lattices has proven to be a highly successful tool with which to realize and study interacting many-body systems in the laboratory [1]. In a typical setup, neutral atoms are loaded with an average density of one per lattice site and interact via contact interactions (Hubbard U), realizing a Fermi- or Bose-Hubbard model [2]. Site-resolved detection in a quantum gas microscope [3,4] and the ability to apply a site-resolved potential [5] add to a rich toolbox to study many-body systems [6]. There are two primary reasons for the focus on densities of around 1: first, because this is the regime corresponding to strongly correlated electrons in condensed matter; and, second and relatedly, because the existing experiments are usually limited to contact interactions, which means that high densities are required to obtain strong interaction effects.

Here, we would like to explore quantum simulation of few-particle systems, i.e., the regime of low densities,

which in turn requires ranged interactions. This is motivated by the ubiquity of long-range forces at the nanoscale [7], which makes it important for fields such as quantum chemistry [8]. Rydberg states are a powerful way to obtain strong-ranged interactions between neutral atoms [9,10], which can also be used for quantum simulation [11,12]. These interactions decay as r^{-6} or r^{-3} [13]. Since the Rydberg interaction is much stronger than hopping, we require Rydberg dressing [14–16] to make the interaction tunable and comparable to hopping rates. This setting, of atoms hopping in a two-dimensional lattice and repelling each other via ranged Rydberg interactions, is reminiscent of electrons in two-dimensional discretized space, albeit with the repulsive force following a different power law than in typical Coulomb interactions. We note that there exist experiments that have successfully explored few-particle physics but with a different focus and context, notably experiments with weakly interacting fermions in the continuum [17–19] or low densities of Rydberg excitations [16,20,21].

Analog quantum chemistry with ultracold atoms has been considered before. The possibility of simulating molecular orbitals has been raised in Ref. [22]. Full analog simulation of quantum chemistry with cold atoms has been proposed in Refs. [23,24]. Although this shows that such an approach is feasible in principle, it is difficult to make it practical with existing technology. Apart from creating three-dimensional potentials and three-dimensional site-resolved detection, another key difficulty in that proposal is the repulsive Coulomb interaction that decays as $1/r$, which requires a cavity and another atomic

*daniel.malz@mpq.mpg.de

†Current address: Department of Physics, Technische Universität München, James-Frank-Straße 1, 85748 Garching, Federal Republic of Germany

Published by the American Physical Society under the terms of the [Creative Commons Attribution 4.0 International license](https://creativecommons.org/licenses/by/4.0/). Further distribution of this work must maintain attribution to the author(s) and the published article's title, journal citation, and DOI.

array to implement. This motivates the search for other platforms (see also Ref. [25]). In the setup proposed here, with Rydberg dressing and in two dimensions, one clearly cannot achieve quantitative agreement with quantum chemistry but, as we show, it is nevertheless possible to simulate what we call “pseudo quantum chemistry,” which is conceptually and qualitatively much like real quantum chemistry. More generally, long-range interactions pose considerable challenges to existing numerical methods, which makes their quantum simulation a particularly worthwhile target.

As we demonstrate with numerics below, in the proposed setup one can reproduce central phenomena of quantum chemistry qualitatively and thus study the physical effects that arise in such systems experimentally. Moreover, the setup is simple and the relevant tools have already been showcased experimentally [26]. Similar to the dense regime (see, e.g., Ref. [27]), this analog quantum simulator can also be used to benchmark classical methods and push the state of the art in classical numerical techniques for interacting few-body problems. Our proposal not only enables pseudo-quantum-chemistry simulations but it also opens up new possibilities in ultracold-atom experiments.

II. SETUP

Our proposal requires fermionic atoms hopping in an optical lattice, with two long-time coherent hyperfine levels that can be dressed to the same Rydberg state (see Fig. 1). We furthermore require a potential with ideally close to single-site resolution, which can be engineered using ac Stark shifts. Shaping of the laser to achieve a tunable potential can be done using, e.g., a digital-mirror device and the objective of a quantum gas microscope [5] or through spatial light modulators [28,29]. For preparation and readout, a quantum gas microscope is essential, because we consider the initial state of the experiments to be atoms localized at known lattice sites.

The Hamiltonian of the system is given through

$$H = H_{\text{kin}} + H_{\text{pot}} + H_{\text{int}}. \quad (1)$$

The noninteracting Hamiltonian, $H_0 = H_{\text{kin}} + H_{\text{pot}}$, comprises the hopping in the lattice and a background potential

$$H_0 = -J \sum_{\langle \vec{i}, \vec{j} \rangle, \sigma} c_{i\sigma}^\dagger c_{j\sigma} - \sum_{\vec{i}, \sigma} V_{\text{pot}, \sigma}(\vec{i}) c_{i\sigma}^\dagger c_{i\sigma}, \quad (2)$$

with hopping rate J and where $c_{i\sigma}^\dagger$ creates a fermion with spin $\sigma \in \{\uparrow, \downarrow\}$, encoded by two hyperfine states of the fermion, on the lattice site i . Note that we allow the potential to be spin dependent in general.

We propose to use Rydberg dressing [14] to engineer repulsive interactions. Using a laser of Rabi frequency Ω and detuning Δ from the transition to a Rydberg state $|r\rangle$,

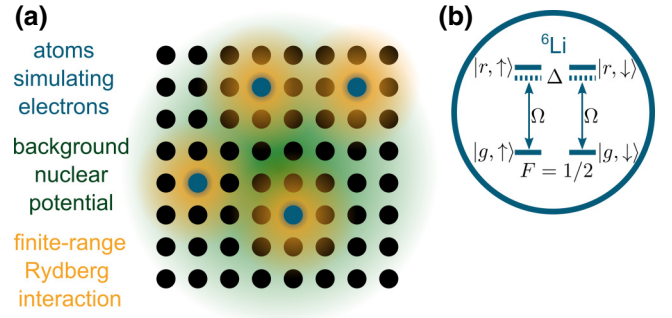


FIG. 1. The proposed setup. (a) Fermionic atoms (blue) with two hyperfine ground states (corresponding to spin-up and spin-down) are trapped in an optical lattice (black). The strength of the trapping laser controls the hopping strength J . The atoms, which play the role of electrons, experience a site-dependent Stark shift that serves to emulate a nuclear potential (green). Repulsive interactions between the atoms are induced through Rydberg dressing (yellow). (b) An example level structure. Rydberg dressing is achieved through a laser of strength Ω that is detuned by Δ from the transition from the $F = 1/2$ hyperfine ground states to a Rydberg state in the p shell.

the ground state of the atom is dressed to $|g\rangle_{dr} \approx |g\rangle + \beta|r\rangle$, with $\beta = \Omega/2\Delta$, where $\Omega \ll \Delta$ (see Fig. 1). The spin degree of freedom can be encoded, for example, in the two states of the $F = 1/2$ hyperfine manifold. In that case, both states can be dressed with a single laser.

At large interatomic distances, this yields a repulsive interaction $V(\vec{r}) \approx \beta^2 V_{\text{ryd}}(\vec{r})$, where \vec{r} is the distance between two dressed atoms and V_{ryd} is the interaction potential for two Rydberg atoms. At small interatomic distances (of the order of a lattice distance), the potential saturates to $\Omega^4/(2|\Delta|)^3$ [16]. The presence of this soft-core potential does not qualitatively change the physics that we explore here but will lead to quantitative differences. For simplicity, in the following we consider an interatomic interaction of the form

$$H_{\text{int}} = V_{\text{int}} \sum_{\vec{i} \neq \vec{j}, \sigma, \rho} \frac{1}{|\vec{i} - \vec{j}|^\alpha} n_{i\sigma} n_{j\rho} + 2V_{\text{int}} \sum_{\vec{i}} n_{i\uparrow} n_{i\downarrow}, \quad (3)$$

where $n_{i\sigma} = c_{i\sigma}^\dagger c_{i\sigma}$ is the number operator and α controls the decay of the interaction. For concreteness and simplicity, we consider just standard Rydberg dressing, which results in interactions that decay with $\alpha = 6$. We note that in the presence of a strong electric field, Rydberg dressing can achieve interactions that decay as $\alpha = 3$ [9,13], which is less commonly implemented but could be interesting for future research, as it is more “long range.”

A. Motivation: Pseudo quantum chemistry

One major motivation to study problems of the type shown in Eq. (1) with low particle density is its similarity

to quantum chemistry. One of the most important problems in quantum chemistry is to find the ground state of N_e electrons in an attractive potential provided by N_{nuc} nuclei, where according to the Born-Oppenheimer approximation, the nuclei are considered immobile [30]. The quantum chemistry Hamiltonian is then composed of the kinetic energy term, the nuclear potential, and the repulsive particle-particle interactions. With this perspective, H_{kin} can be interpreted as the motion of electrons in two-dimensional discretized space and H_{int} as the Coulomb repulsion (albeit with a different power-law decay), while the background potential can be chosen as

$$H_{\text{pot}} = H_{\text{nuc}} = - \sum_{\vec{i}} \sum_n V_{\text{nuc}}^{(n)}(\vec{i}) c_i^\dagger c_i, \quad (4)$$

where $V_{\text{nuc}}^{(n)}(\vec{r}) = V_0 Z_n / (|\vec{r}_n - \vec{r}|)$ is the attractive potential produced by the n^{th} nucleus. We assume that there are N_{nuc} nuclei, placed at positions \vec{r}_n and with charge Z_n . We parametrize the strength of the nuclear potential as $V_0 = J/a_0$, where a_0 sets the Bohr radius in units of the lattice constant and thus the Rydberg constant $\text{Ry} = J/a_0^2$.

We note that a r^{-1} nuclear potential is not strictly required to see phenomena akin to quantum chemistry and that qualitatively similar physics can be observed in a variety of nuclear potential shapes. The two-dimensional geometry allows essentially arbitrary on-site potential to be applied from the transverse direction. This leaves considerable freedom in choosing a nuclear potential. Natural choices are $V_{\text{nuc}}(r) \propto \log(r)$, which is the electromagnetic potential in flatland consistent with Gauss's law, or $V_{\text{nuc}}(r) \propto r^{-\alpha}$ for integer α .

The flatland potential $V_{\text{nuc}}(r) \propto \log(r)$ has been investigated in Ref. [31]. This potential obeys Gauss's law in two dimensions, which means that if the "electrons" could be made to interact according to the same potential, then at large distances, a two-dimensional atom would appear to have a charge equal to the coordination number minus the number of bound electrons. However, since Rydberg dressing can only produce interactions that scale as r^{-3} or r^{-6} , we have to sacrifice Gauss's law.

It therefore makes sense to go to a more localized nuclear potential as well, which improves convergence with system size and makes it easier to have strong interactions. It is tempting to choose $V_{\text{nuc}}(r) \propto r^{-\alpha}$ with $\alpha = 3$ or $\alpha = 6$ to match it to the electronic interaction potential. However, an attractive potential with $\alpha \geq 2$ leads to a Hamiltonian that is not lower bounded. This can easily be seen by inserting a trial wave function $\psi(r) = \exp(-r^2/(2\sigma^2))/\sqrt{\pi\sigma^2}$ into the Hamiltonian, which yields

$$\langle \psi | H | \psi \rangle = \int_0^\infty \frac{2\pi r dr}{\pi\sigma^2} e^{-r^2/\sigma^2} \left(-r^{-\alpha} + \frac{2}{\sigma^2} - \frac{r^2}{\sigma^4} \right). \quad (5)$$

While the kinetic energy is finite, the integral giving the potential energy only converges for $\alpha < 2$.

Thus, as a compromise, we propose to use $V_{\text{nuc}}(r) = -V_0/r$. The system can then be interpreted as a standard atom but with the electron confined to move in a plane. In this scenario, we can identify $V_0 = e^2/(4\pi\epsilon_0)$. This potential has the advantage that the single-particle wave functions can be obtained analytically through standard procedure [32]. With the present choice, the nuclear potential can be interpreted as being generated by a Coulomb force in three dimensions but with the electron confined to move in a plane. In this scenario, we can identify $V_0 = e^2/(4\pi\epsilon_0)$ and one can find the atomic orbitals analytically in the continuum [32], with principal energies $E_n = -\text{Ry}/(n - 1/2)^2$. A more experimentally friendly choice could be a Gaussian potential produced by a tightly focused laser beam.

We note that the Hamiltonian $H = H_0 + H_{\text{int}}$ does not include spin-orbit coupling; it does not couple spin-up to spin-down particles. Nevertheless, spin is explicitly included and has important consequences, as we explore below. Furthermore, H_{pot} could include a linear gradient, which would model an electric field (a potential gradient coupling independent of spin) or a gradient with opposite signs for spin-up and spin-down particles, which corresponds to an applied magnetic field.

In the following, we focus on the pseudo-quantum-chemistry regime for concreteness and so we take the background potential to be the nuclear potential produced by some distribution of nuclei as specified in Eq. (4). In general, a large Bohr radius a_0 is preferred to make connection to the continuum limit (see, e.g., the discussion in Ref. [24]) but this comes at the cost of more stringent experimental (and numerical) requirements. Specifically, a larger Bohr radius leads to a smaller Rydberg constant Ry , which means that preparation takes longer, giving more time for decoherence to act. Moreover, larger orbits make disorder in the nuclear potential more problematic. We make the choice $a_0 = 2$ for most of the plots, as this leads to time scales that are already accessible with current experimental parameters. We fix the strength of the repulsive potential such that at a distance of one Bohr radius, the nuclear attraction is equal to the electronic repulsion. This leads to $V_{\text{int}} = J a_0^{\alpha-2}/\alpha$. We also take $\alpha = 6$.

B. Preparation and measurement

To find the ground-state energy requires preparation of the ground state with high fidelity and subsequent measurement of its energy. We propose to prepare the ground state adiabatically. There is substantial freedom in designing adiabatic paths. Here, we propose to take the simplest choice: first prepare the noninteracting electronic state and then adiabatically turn on interactions. This has the advantage that for the majority of the time, the interaction (and

thus Rydberg decay) is turned off. Starting with exactly N_e atoms, localized at known sites in the optical lattice, and no hopping, first prepare the desired spin state, which can be done using the single-site access afforded by a quantum gas microscope [33]. Second, tune the noninteracting Hamiltonian H_0 adiabatically to its final form. This requires a Hamiltonian path that takes the wave function of the N_e electrons on their initial sites (which are eigenstates when hopping is turned off) to the desired molecular orbitals. In a final step, turn on interactions adiabatically to reach the interacting ground state.

To understand how the adiabatic preparation time generally depends on the Bohr radius a_0 , note that the gaps between the atomic orbitals are proportional to the Rydberg constant $\text{Ry} = J/a_0^2$, which intuitively corresponds to the rate at which an atom can explore an area equal to an orbital of radius a_0 . Since adiabatic preparation generally scales with the inverse of the gap squared [34], we expect that the adiabatic preparation time scales as $\text{Ry}^{-2} \propto a_0^4$.

To measure the preparation fidelity, perhaps the simplest approach is to reverse the adiabatic preparation and then to measure the particle distribution. To a good approximation, the probability for the atoms to return to their initial positions is the square of the fidelity of the ground-state preparation.

Rather than measuring the occupancy of the ground state, it is also possible to measure the energy of the system directly. This requires measuring the kinetic and potential energy of the atoms. The potential energy can be computed straightforwardly from the atomic configuration in real space and thus measuring it requires taking a snapshot of the system with a quantum gas microscope. The kinetic energy requires determining the momentum of each particle, which may be done using time-of-flight detection, provided that all atoms can be caught. Such single-atom momentum measurements have already been realized [18,35,36].

Finally, below we also discuss the potential for doing spectroscopy directly on the system.

C. Experimental imperfections

Rydberg dressing leads to the main source of decoherence for this protocol, because the admixed Rydberg state may decay [15]. Given a dressing $|g\rangle_{dr} = |g\rangle + \beta|r\rangle$, the interaction at large distances scales with β^4 , whereas the probability of a Rydberg decay scales as β^2 . Since we require $\beta \ll 1$ to make the hopping and Rydberg interaction rates comparable, the ratio of interaction strength to decay rate is multiplied by a small factor β^2 relative to the equivalent ratio of the Rydberg state. If an atom is excited to the Rydberg state, it is typically lost rapidly, as is observed in experiment [16,26], which is why in the experiments one can postselect onto runs in which the atom number remains unchanged to remove this effect.

However, this still leads to a limitation, as the success probability of the experiment decays exponentially with time, which means that Rydberg decay effectively limits the accessible time scales. Thus, the main focus of our numerical simulations is to assess whether the adiabatic preparation can succeed within the time available.

In Ref. [26], Rydberg dressing has resulted in a lifetime of about $\tau_{\text{eff}} = 1$ ms at an interaction strength comparable to the hopping of $J = 2\pi \times 1.7$ kHz, leading to a figure of merit of about $J\tau_{\text{eff}} \approx 10$. We note that the widely observed avalanche loss [15,16,37,38] can be neglected in this experimental setting, for two reasons. First, it has been experimentally found to be almost negligible at small densities [26]. Second, even if present, avalanche loss does not alter the probability that all atoms survive, as it only acts after the first Rydberg excitation has occurred. Below, we show that even in a time of about $10J^{-1}$, the interacting ground state of simple systems can be prepared with fairly high fidelity (*cf.* Fig. 2), placing the experiments proposed here within experimental reach.

Other experimental imperfections include disorder in the nuclear potential, which arises because the optical lattice spacing is comparable to or below the diffraction limit, which makes it difficult to implement the potential accurately. Any experiment will also have errors in the preparation of the initial state as well as measurement errors. These errors can be accounted for by multiplying the corresponding fidelities to those we report in Fig. 2. Finally, as in all ultracold-atom experiments, collisions with background gas and heating through laser fluctuations must be controlled sufficiently as to not influence the experiment during the preparation and simulation time.

III. RESULTS

In this section, we numerically simulate a few potential near-term experiments using exact diagonalization. Exact classical simulation of the system is expensive and so we are limited to small system sizes and few atoms.

A. Adiabatic preparation of pseudoatoms and pseudomolecules

We explore adiabatic preparation through the examples of two fermions in one or two potential sites, analogous to helium and molecular hydrogen. The most stringent experimental limitation may be Rydberg decay, which limits the total achievable interaction time. Running adiabatic preparation in finite time leads to errors and this is why in the following we assess how well adiabatic preparation can succeed using only ten (or in one case 20) hopping times. We study both the case in which the two particles are in a spin singlet (corresponding to the actual ground state), in which case they behave like bosons, and the case in which they are in a spin triplet (e.g., both in the same hyperfine ground state), where they behave like fermions.

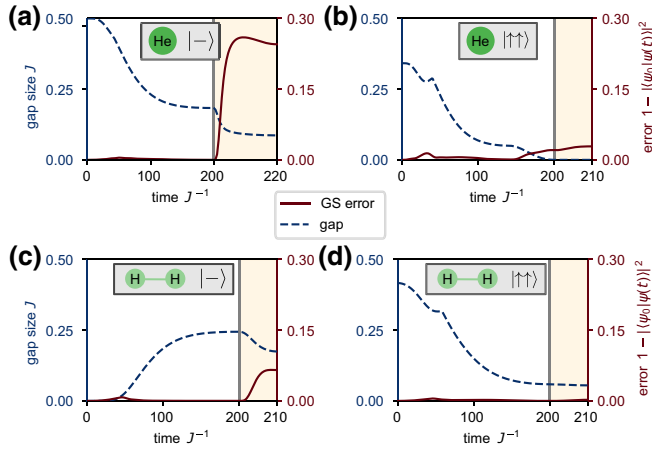


FIG. 2. The adiabatic preparation of pseudo-He and H_2 . We illustrate the adiabatic preparation by the example of He and H_2 . At $t = 0$, we start with two fermions in (a),(c) a spin singlet $|-\rangle$ or (b),(d) a triplet $|\uparrow\uparrow\rangle$. The adiabatic preparation proceeds by preparing the noninteracting ground state up to $t = 200J^{-1}$ (vertical gray line) and subsequently turning on the interaction adiabatically (yellow-shaded area). For details on the preparation, we refer to the main text. The system parameters used to simulate the preparation of He are $a_0 = 4$ and central charge $Z = 2$, with the nucleus placed in the center of a 21×21 lattice. For H_2 , we separate two nuclei with $Z = 1$, $a_0 = 2$ by three lattice sites and center them in a 24×21 lattice. As interactions, we always take $\alpha = 6$ and $V_{\text{int}} = Ja_0^{\alpha-2}/\alpha$. Note that in (a), for bosons in He, the interaction time is twice as long as in the other panels. The shown errors for the wave function lead to relative errors in the ground-state energy prediction of about (a) 47%, (b) 2.4%, (c) 3.7%, and (d) 0.1%. Note that in all panels, the interacting region $Jt > 200$ is stretched for presentation reasons.

The conceptually simplest case is bosonic helium [Fig. 2(a)], because both particles occupy the same orbital. In our simulations, we assume that there is a single nucleus with $Z = 2$ in the middle of a $(2p + 1) \times (2p + 1)$ lattice and place both particles on the same site. In all simulations here, the padding $p = 10$. This initial state is the unique ground state of the Hamiltonian given in Eq. (1) with both hopping and interactions turned off. With the nuclear potential fixed, we smoothly turn on hopping $J(t) = J \sin^2(\pi t/(2T))$ from $t = 0$ to $t = T$ with $T = 200J^{-1}$, which prepares both particles in the $1s$ orbital. Subsequently, we similarly turn on interactions $V_{\text{int}}(t) = V_{\text{int}} \sin^2(\pi(t - T)/(2(T + T_{\text{int}})))$, from $t = T$ to $t = T + T_{\text{int}}$, with $T_{\text{int}} = 10$, while keeping H_0 fixed. Out of the four systems that we explore in Fig. 2, the preparation fidelity in Fig. 2(a) is by far the worst. The reason is that in the noninteracting state, the two particles are in the same orbital, closely bound to the nucleus. The repulsive interaction thus causes a large change in the wave function. The chosen interaction time of $20J^{-1}$ is too short for the ground state to adiabatically follow the change. Numerically, we find that the interaction time required to get an error well below 10% is around $100J^{-1}$.

Helium with electrons in the triplet state [Fig. 2(b)] is somewhat more complicated, as the noninteracting part requires us to simultaneously prepare one particle in the $1s$ orbitals and one in an excited orbital. To prepare this state, we place one particle on the nucleus site and a second particle three sites away and add another auxiliary nuclear potential on that site, at 90% of the strength of the original one, such that this site has the second-lowest potential. In a two-step process, we first turn on hopping while keeping this potential configuration fixed (same $J(t)$ as above but with $T = 140J^{-1}$) and then adiabatically turn off the auxiliary nuclear potential. Note that in the absence of the auxiliary nuclear potential, the first excited state of the system is degenerate, corresponding to two $2p$ orbitals. Note that while this would usually lead to a breakdown of adiabaticity, it does not do so here, because the matrix element between the two states is zero due to symmetry. In the last step, we turn on interactions adiabatically while turning off V_{2p} .

The preparation of molecular hydrogen [Figs. 2(c) and 2(d)] is conceptually more straightforward. We always start with one particle on each of the two nuclei sites, turn on hopping adiabatically, and then turn on interactions.

At this stage, the particle statistics already play a very important role. If we initialize the system in a spin singlet, the spatial wave function is symmetric (bosonic) and both particles occupy the same orbital. The particles spend a lot of time near each other and, consequently, turning on repulsive interactions has a large effect on the wave functions. Clearly, this affects helium more than H_2 , as the lowest orbital in He is more confined than in H_2 . If we instead initialize the system in a symmetric spin-triplet state, the particles behave like fermions and are already well separated on average and thus additional repulsive interactions hardly change the state.

B. Example two-dimensional chemistry experiment: Molecular hydrogen

With the ability to prepare the ground state of molecular hydrogen, we now explore how well bond length and ground-state energy can be found with limited interaction time. To this end, we simulate the adiabatic preparation for a range of nucleus separations and interaction times T_{int} . The results are shown in Fig. 3.

Our results indicate that even in a modest interaction time such as $T_{\text{int}} = 10J^{-1}$, one can already clearly see the molecular bound state and obtain an accurate result for the bond length. Again, we also observe a clearly observable difference between fermionic and bosonic particles. The bosonic case is qualitatively much as one would expect, with a clearly defined molecular potential, even for short interaction times. At short to intermediate distances, quantitative agreement with the true value is reached at still modest times between $20J^{-1}$ and $40J^{-1}$. Interestingly,

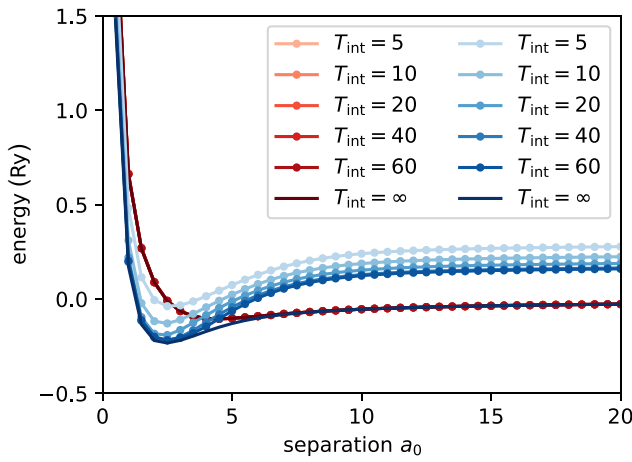


FIG. 3. The simulated experimental determination of the binding energy and bond length of pseudo- H_2 . We simulate the adiabatic preparation of the ground states of pseudo- H_2 for a range of nucleus separations and for either bosonic (blue) or fermionic particles (red). We plot the predicted ground-state energy minus twice the energy of H (corresponding to free hydrogen atoms). In a symmetric spin-triplet state (red), the atoms have an anti-symmetric spatial wave function, such that they occupy different orbitals, and thus the interaction hardly has any effect (the curves all lie on top of each other). The molecule is very weakly bound in this case (hardly visible). In the actual ground state of H_2 , the electrons are in a spin singlet and the optimal bond length is clearly visible, even at very short preparation times. At large separations, the adiabatic preparation increasingly fails to produce the correct energy, as overlap of the single-particle wave functions decays exponentially with distance. Parameters: $a_0 = 2$, padding $p = 10$, and $V_{\text{int}} = a_0^{\alpha-2}/\alpha$.

there is evidently also a limitation of our chosen adiabatic path, in that it fails to give the right ground state at large separations. The reason is that in the initial noninteracting ground state, both particles occupy a symmetric orbital across both nuclei, which yields a 50% chance of finding both particles on the same nucleus. Clearly, the true ground state at large separations should be two isolated hydrogen atoms, with zero probability of finding both particles at the same nucleus. However, at large distances there is a potential barrier for particles to move between the nuclei, leading to exponentially small matrix elements between the states, which makes the adiabatic preparation fail.

In contrast, the molecular potential for fermionic particles hardly exists, to the extent that it is not properly visible in the plot. In this case, there is no issue with also obtaining the ground state adiabatically at large separations, because the noninteracting ground state is already correct in that case.

C. Spectroscopy

In real atoms, coupling to the electromagnetic field allows excited electrons to relax to the ground state and coherent driving yields Rabi oscillations. In the dipole

approximation, the atom is taken to be small as compared to the wavelength of the emitted light. In the present context, we can model coherent driving by applying a oscillating linear background potential, which allows us to observe dipole transitions. In this section, we focus on the noninteracting problem for simplicity. Experimentally, the interacting case works just as well as the noninteracting case but the times required to perform spectroscopy demand about one-order-of-magnitude improvements on the previously reported figure of merit of the Rydberg-dressing time over the Rydberg-decay time. Spectroscopy through modulation of the optical lattice has been employed several times in the many-body regime, where instead of Rabi oscillations, one can measure frequency-dependent heating rates [39,40].

Specifically, we simulate the Hamiltonian $H = H_0 + g \sin(\omega t)H_{\text{lin}}(t)$ with

$$H_{\text{lin}}(t) = \frac{1}{a_0} \sum_{\vec{i}} (i_x - N/2) c_{i\sigma}^\dagger c_{i\sigma}. \quad (6)$$

In order to see clean Rabi oscillations, we should set ω close to the frequency of a dipole-allowed transition—say, $\omega_{21} = \omega_{2p} - \omega_{1s}$ —and drive weakly enough that transitions to other states are suppressed by the detuning to them. To understand these conditions, note that the principal energy levels have approximately the energy [32]

$$E_n = -\frac{\text{Ry}}{(2n-1)^2} = -\frac{J}{a_0^2(2n-1)^2}, \quad (7)$$

where $\text{Ry} = V_0^2/J = J/a_0^2$ is the Rydberg constant, a_0 is the Bohr radius in units of the lattice constant, and J is the hopping strength. These energies are exact in the continuum $a_0 \rightarrow \infty$ but the quality of approximation in finite systems and with finite a_0 depends on the chosen orbital. Nevertheless, they provide a good guide. To get clean Rabi oscillations, the coupling must be weak. For example, if we drive the transition from $1s$ to $2p$, the detuning to the $1s$ - $3p$ transition is $J(1/9 - 1/25)/a_0^2 \approx 0.07J/a_0^2$. The matrix elements $\langle 2p|H_{\text{lin}}|1s\rangle$ and $\langle 3p|H_{\text{lin}}|1s\rangle$ depend somewhat on a_0 but are roughly of order 1. Thus, we need $g \ll 0.1J/a_0^2$ to see Rabi oscillations. Higher transitions are increasingly difficult to observe, because they require weaker coupling. For this reason, we choose $a_0 = 1$ (small electron orbits), as this leads to shorter experiments.

We model spectroscopy numerically in the following way. We initialize the system in the ground state of hydrogen (one electron in the $1s$ orbital) and apply the oscillating Hamiltonian $H_0 + g \sin(\omega t)H_{\text{lin}}(t)$ [see Eq. (6)] for a time t . We then detect the probability that the system will remain in the electronic ground state by first applying the inverse of the adiabatic preparation and then checking whether the atom returns to the initial lattice site. This reduces the problem of detecting the ground-state probability to measuring

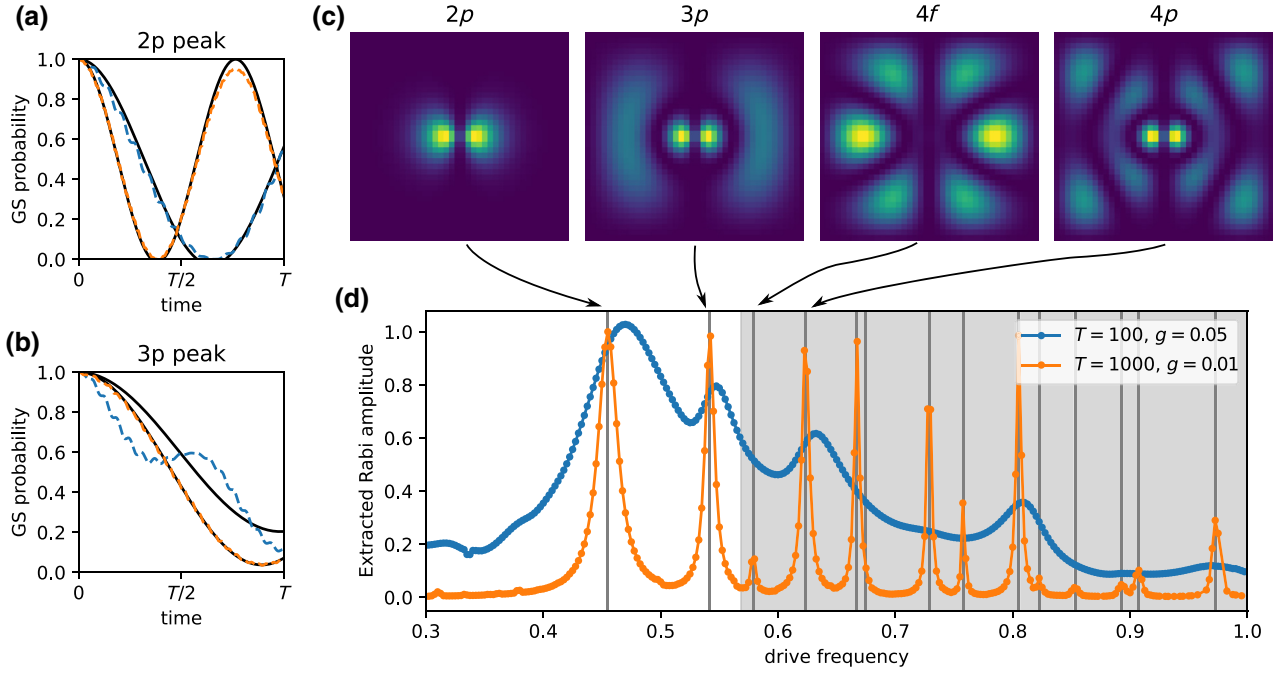


FIG. 4. The spectroscopy of hydrogen. Starting from a particle in the $1s$ orbital, an oscillating linear field is applied, corresponding to coherent driving in the dipole approximation. The resulting dynamics are monitored by measuring the ground-state probability as a function of time. We simulate this process on a 40×38 lattice (to break symmetry for convenience) for a range of drive frequencies from $\omega = 0$ to $\omega = J$ once for a driving strength $g = 0.05$ and a total time of $T = 100/J$ (blue) and once for a driving strength $g = 0.01$ and a total time $T = 1000/J$ (orange). We choose a small Bohr radius $a_0 = 1$ such that we can use a larger g and shorter times. At each frequency, we fit $1 - A \sin^2(\Omega t)$ to the numerically calculated ground-state probability $|c_0(t)|^2$. (a) The time trace of the first resonance, which corresponds to the $1s$ - $2p$ transition. We plot the numerically calculated ground-state probability (dashed colored line) and the fit (solid black line). Note that the x axis is scaled to the total time, which is $100/J$ (blue) and $1000/J$ (orange). (b) The same plot for the $1s$ - $3p$ transition. The blue curve deviates markedly from a pure sine function, as the effective coupling is fairly strong compared to the detuning to other states. (c) Orbital wave functions of the excited states corresponding to the spectroscopy peaks. (d) A plot of the fitted Rabi amplitude A as a function of the drive frequency. Weaker coupling requires longer times but leads to a better resolution of the peaks. Note that the $1s$ - $4f$ transition is forbidden but since the system does not obey rotation symmetry exactly, there exists a small nonzero matrix element. The gray-shaded area corresponds to transitions to states with an energy greater than $-4J$ (which in the infinite system would correspond to an unbound electron). The energy of these states is dominated by the confinement to a finite lattice rather than the bound-state component.

the probability that the atom is localized at a specific site. We repeat this process for different times from 0 to a total time T . Given sufficiently weak driving, the system will undergo oscillations if the drive frequency is tuned to an electronic transition and otherwise will remain mostly in the ground state. We then sweep the drive frequency and record the amplitudes of the observed Rabi amplitudes to detect the resonances of the system. The result is shown in Fig. 4.

IV. EXPERIMENTAL IMPLEMENTATION

Our proposal requires fermionic atoms that can be trapped in an optical lattice, imaged with single-site resolution, Rydberg dressed, and that have at least two long-time coherent hyperfine levels (see Fig. 1). These are all state-of-the-art capabilities and several atomic species could serve this purpose. Standard choices are the alkali atoms

^{40}K or ^6Li . Alkaline-earth(-like) atoms have a number of favorable optical properties, such as ultranarrow-line-width transitions, that have enabled their use as clocks [41] and for quantum simulation [42], and make them promising candidates for quantum computing [43]. Among the most common fermionic species are ^{87}Sr , ^{171}Yb , and ^{173}Yb . Recently, coherent gates for individual (pairs of) ^{171}Yb atoms have been achieved with high fidelity, exploiting the high coherence time of the nuclear spin [44]. Other common species such as ^{87}Sr [43,45] may be equally suitable. Proof-of-principle experiments of up to two electrons could also be done with bosons such as ^{87}Rb .

The key figure of merit for experiments is the ratio of the hopping rate divided by the effective Rydberg-decay rate, $M = J/\Gamma$. It can be interpreted as the number of sites that an atom can explore before decaying. We note that to measure the energy of the state or the overlap

with the ground state, all atoms have to be detected at the end of the experiment, which naturally leads to post-selection onto runs in which no atoms have decayed. Note that avalanche loss [15,16,37,38], whether present or not, does not affect the probability of all atoms remaining, as it only acts after the first atom has decayed. Preparation of the ground states of larger molecules requires longer times or approaching the continuum limit by increasing a_0 requires longer simulation times, which will translate to low success probabilities unless M is sufficiently large.

To maximize M , the hopping J must be large and Rydberg decay Γ must be slow. Thus, it is favorable to use a light atomic species with fast hopping, such as ${}^6\text{Li}$, as has been done in Ref. [26]. Rydberg decay can be suppressed by dressing with Rydberg states of higher principal quantum number n . Generally, the lifetime of low-angular-momentum Rydberg states including black-body radiation scales as n^3 . In contrast, the strength of the interactions scales as n^4 . Thus, since we use Rydberg dressing to obtain an interaction strength comparable to hopping, we scale $\beta \propto n^{-1}$, such that $V_{\text{int}} \propto n^4 \beta^{-4} = \text{const}$. As a result, the Rydberg-decay rate relative to the hopping strength scales as $\Gamma \propto n^{-3} \beta^2 \propto n^{-5}$. Using this scaling, we obtain that dressing to $n = 70$ instead of $n = 28$ as in Ref. [26] would lead to a 100-fold improvement in M .

Another potential approach to reduce the Rydberg-decay rate while maintaining the same effective interaction strength is stroboscopic dressing [46]. If the dressing is turned on and off at a rate much larger than other relevant time scales, it is well approximated by continuous dressing but with the values for β^2 and β^4 replaced by their time-averaged values. If we assume for simplicity that dressing is on for a fraction η of the time and otherwise off, we find that to keep the same effective interaction strength, we need to increase $\beta \rightarrow \beta_\eta = \beta \eta^{-1/4}$. However, the induced Rydberg decay will then be reduced $\Gamma \rightarrow \Gamma_\eta = \Gamma \eta^{1/2}$, such that $M \propto \eta^{1/2}$.

Finally, it would be worth exploring how weak the optical lattice can be before problematic effects appear. For example, the standard condition is that next-to-nearest-neighbor hopping must be negligible but this is perhaps not strictly necessary here, especially since in real atoms and molecules there is a relativistic correction to the kinetic energy of approximately p^4 , which would be generated through next-to-nearest interactions. In principle, the scheme presented here could in principle even work in the continuum, although it is not clear how exactly one would control the kinetic energy term and implement the nuclear potential.

V. CONCLUSIONS

We show that Rydberg dressing in standard ultracold-lattice-atom experiments allows for the simulation of

pseudo quantum chemistry, which differs from real quantum chemistry by being two-dimensional and having a different scaling law for the Coulomb interaction. Nevertheless, pseudo quantum chemistry inherits key phenomenology from quantum chemistry, including (anti)bonding orbitals and the potential for spectroscopy. The key experimental figure of merit that determines how well such simulations can be done is the ratio of the Rydberg-decay rate to the hopping strength. We show, using parameters from existing experiments, that current experiments can already prepare the ground state of small molecules. Since it is realistic for the figure of merit to increase substantially in the future, this motivates the use of this platform to explore quantum chemistry physics experimentally, to gain insights into complex electronic processes, and to benchmark classical codes.

Future work should explore how spin-orbit interactions or other important corrections (e.g., relativistic corrections) could be added to the simulator. Moreover, the adiabatic paths used in our numerical simulation can likely be improved, especially when tailored to given specific experimental capabilities. Also, we have hardly explored $\alpha = 3$, which may feasibly be obtained through Rydberg dressing and could be advantageous as the resulting interactions are stronger, which could result in a larger hopping to decay-rate ratio. It would also be interesting to go more into detail about the physics, which differs from normal quantum chemistry. An obvious example is that neither the nuclear potential nor the electronic repulsion obey Gauss's law, which means that in principle arbitrarily many electrons could fit around a nucleus.

Going beyond the analogy with quantum chemistry, it would be interesting to understand how the physics of this platform is modified in the presence of additional interactions, disorder, or unavoidable dissipation. Finally, the few-body low-density regime of ultracold-atom experiments may yield other fruitful research directions. For example, when the repulsive interaction dominates the kinetic energy term and the atoms are sufficiently dense, the ground-state configuration ought to be related to packing of circles in two dimensions. These configurations can also be obtained adiabatically.

ACKNOWLEDGMENTS

We thank Pascal Weckesser and Simon Hollerith for helpful discussions about experimental considerations. We acknowledge funding from European Research Council Advanced Grant ‘‘Quantum Emitters in Non-Conventional Baths’’ (QUENOCOBA) under the European Union Horizon 2020 program (Grant Agreement No. 742102). This research is part of the Munich Quantum Valley, which is supported by the Bavarian state government with funds from the Hightech Agenda Bayern Plus.

- [1] I. Bloch, J. Dalibard, and W. Zwerger, Many-body physics with ultracold gases, *Rev. Mod. Phys.* **80**, 885 (2008).
- [2] D. Jaksch, C. Bruder, J. I. Cirac, C. W. Gardiner, and P. Zoller, Cold Bosonic Atoms in Optical Lattices, *Phys. Rev. Lett.* **81**, 3108 (1998).
- [3] W. S. Bakr, J. I. Gillen, A. Peng, S. Fölling, and M. Greiner, A quantum gas microscope for detecting single atoms in a Hubbard-regime optical lattice, *Nature* **462**, 74 (2009).
- [4] E. Haller, J. Hudson, A. Kelly, D. A. Cotta, B. Peaudecerf, G. D. Bruce, and S. Kuhr, Single-atom imaging of fermions in a quantum-gas microscope, *Nat. Phys.* **11**, 738 (2015).
- [5] J. Y. Choi, S. Hild, J. Zeiher, P. Schauß, A. Rubio-Abadal, T. Yefsah, V. Khemani, D. A. Huse, I. Bloch, and C. Gross, Exploring the many-body localization transition in two dimensions, *Science* **352**, 1547 (2016).
- [6] C. Gross and I. Bloch, Quantum simulations with ultracold atoms in optical lattices, *Science* **357**, 995 (2017).
- [7] R. H. French, *et al.*, Long range interactions in nanoscale science, *Rev. Mod. Phys.* **82**, 1887 (2010).
- [8] B. Bauer, S. Bravyi, M. Motta, and G. K.-L. Chan, Quantum algorithms for quantum chemistry and quantum materials science, *Chem. Rev.* **120**, 12685 (2020).
- [9] D. Jaksch, J. I. Cirac, P. Zoller, S. L. Rolston, R. Cote, and M. D. Lukin, Fast Quantum Gates for Neutral Atoms, *Phys. Rev. Lett.* **85**, 2208 (2000).
- [10] M. D. Lukin, M. Fleischhauer, R. Cote, L. M. Duan, D. Jaksch, J. I. Cirac, and P. Zoller, Dipole Blockade and Quantum Information Processing in Mesoscopic Atomic Ensembles, *Phys. Rev. Lett.* **87**, 037901 (2001).
- [11] H. Weimer, M. Müller, I. Lesanovsky, P. Zoller, and H. P. Büchler, A Rydberg quantum simulator, *Nat. Phys.* **6**, 382 (2010).
- [12] A. Browaeys and T. Lahaye, Many-body physics with individually controlled Rydberg atoms, *Nat. Phys.* **16**, 132 (2020).
- [13] G. Pupillo, A. Micheli, M. Boninsegni, I. Lesanovsky, and P. Zoller, Strongly Correlated Gases of Rydberg-Dressed Atoms: Quantum and Classical Dynamics, *Phys. Rev. Lett.* **104**, 223002 (2010).
- [14] I. Bouchoule and K. Mølmer, Spin squeezing of atoms by the dipole interaction in virtually excited Rydberg states, *Phys. Rev. A* **65**, 041803 (2002).
- [15] J. B. Balewski, A. T. Krupp, A. Gaj, S. Hofferberth, R. Löw, and T. Pfau, Rydberg dressing: Understanding of collective many-body effects and implications for experiments, *New J. Phys.* **16**, 063012 (2014).
- [16] J. Zeiher, R. van Bijnen, P. Schauß, S. Hild, J. Yoon Choi, T. Pohl, I. Bloch, and C. Gross, Many-body interferometry of a Rydberg-dressed spin lattice, *Nat. Phys.* **12**, 1095 (2016).
- [17] L. Bayha, M. Holten, R. Klemt, K. Subramanian, J. Bjerlin, S. M. Reimann, G. M. Bruun, P. M. Preiss, and S. Jochim, Observing the emergence of a quantum phase transition shell by shell, *Nature* **587**, 583 (2020).
- [18] M. Holten, L. Bayha, K. Subramanian, C. Heintze, P. M. Preiss, and S. Jochim, Observation of Pauli Crystals, *Phys. Rev. Lett.* **126**, 020401 (2021).
- [19] M. Holten, L. Bayha, K. Subramanian, S. Brandstetter, C. Heintze, P. Lunt, P. M. Preiss, and S. Jochim, Observation of Cooper pairs in a mesoscopic two-dimensional Fermi gas, *Nature* **606**, 287 (2022).
- [20] H. Bernien, S. Schwartz, A. Keesling, H. Levine, A. Omran, H. Pichler, S. Choi, A. S. Zibrov, M. Endres, M. Greiner, V. Vuletić, and M. D. Lukin, Probing many-body dynamics on a 51-atom quantum simulator, *Nature* **551**, 579 (2017).
- [21] S. Hollerith, J. Zeiher, J. Rui, A. Rubio-Abadal, V. Walther, T. Pohl, D. M. Stamper-Kurn, I. Bloch, and C. Gross, Quantum gas microscopy of Rydberg macrodimers, *Science* **364**, 664 (2019).
- [22] D.-S. Lühmann, C. Weitenberg, and K. Sengstock, Emulating Molecular Orbitals and Electronic Dynamics with Ultracold Atoms, *Phys. Rev. X* **5**, 031016 (2015).
- [23] J. Argüello-Luengo, A. González-Tudela, T. Shi, P. Zoller, and J. I. Cirac, Analogue quantum chemistry simulation, *Nature* **574**, 215 (2019).
- [24] J. Argüello-Luengo, A. González-Tudela, T. Shi, P. Zoller, and J. I. Cirac, Quantum simulation of two-dimensional quantum chemistry in optical lattices, *Phys. Rev. Res.* **2**, 042013 (2020).
- [25] J. Knörzer, C. J. van Diepen, T.-K. Hsiao, G. Giedke, U. Mukhopadhyay, C. Reichl, W. Wegscheider, J. I. Cirac, and L. M. K. Vandersypen, Long-range electron-electron interactions in quantum dot systems and applications in quantum chemistry, *Phys. Rev. Res.* **4**, 033043 (2022).
- [26] E. Guardado-Sanchez, B. M. Spar, P. Schauss, R. Belyan-sky, J. T. Young, P. Bienias, A. V. Gorshkov, T. Iadecola, and W. S. Bakr, Quench Dynamics of a Fermi Gas with Strong Nonlocal Interactions, *Phys. Rev. X* **11**, 021036 (2021).
- [27] B. H. Madhusudhana, S. Scherg, T. Kohlert, I. Bloch, and M. Aidelsburger, Benchmarking a Novel Efficient Numerical Method for Localized 1D Fermi-Hubbard Systems on a Quantum Simulator, *PRX Quantum* **2**, 1 (2021).
- [28] A. L. Gaunt and Z. Hadzibabic, Robust digital holography for ultracold atom trapping, *Sci. Rep.* **2**, 721 (2012).
- [29] M. R. Sturm, M. Schlosser, R. Walser, and G. Birkl, Quantum simulators by design: Many-body physics in reconfigurable arrays of tunnel-coupled traps, *Phys. Rev. A* **95**, 063625 (2017).
- [30] A. Aspuru-Guzik, A. D. Dutoi, P. J. Love, and M. Head-Gordon, Simulated quantum computation of molecular energies, *Science* **309**, 1704 (2005).
- [31] O. Atabek, C. Deutsch, and M. Lavaud, Schrödinger equation for the two-dimensional Coulomb potential, *Phys. Rev. A* **9**, 2617 (1974).
- [32] B. Zaslav and M. E. Zandler, Two-dimensional analog to the hydrogen atom, *Am. J. Phys.* **35**, 1118 (1967).
- [33] C. Gross and W. S. Bakr, Quantum gas microscopy for single atom and spin detection, *Nat. Phys.* **17**, 1316 (2021).
- [34] T. Albash and D. A. Lidar, Adiabatic quantum computation, *Rev. Mod. Phys.* **90**, 15002 (2018).
- [35] H. Cayla, C. Carcy, Q. Bouton, R. Chang, G. Carleo, M. Mancini, and D. Clément, Single-atom-resolved probing of lattice gases in momentum space, *Phys. Rev. A* **97**, 061609 (2018).
- [36] C. Carcy, H. Cayla, A. Tenart, A. Aspect, M. Mancini, and D. Clément, Momentum-Space Atom Correlations in a Mott Insulator, *Phys. Rev. X* **9**, 041028 (2019).
- [37] E. A. Goldschmidt, T. Boulier, R. C. Brown, S. B. Koller, J. T. Young, A. V. Gorshkov, S. L. Rolston,

- and J. V. Porto, Anomalous Broadening in Driven Dissipative Rydberg Systems, *Phys. Rev. Lett.* **116**, 113001 (2016).
- [38] L. Festa, N. Lorenz, L.-M. Steinert, Z. Chen, P. Osterholz, R. Eberhard, and C. Gross, Blackbody-radiation-induced facilitated excitation of Rydberg atoms in optical tweezers, *Phys. Rev. A* **105**, 013109 (2022).
- [39] T. Stöferle, H. Moritz, C. Schori, M. Köhl, and T. Esslinger, Transition from a Strongly Interacting 1D Superfluid to a Mott Insulator, *Phys. Rev. Lett.* **92**, 130403 (2004).
- [40] R. Jördens, N. Strohmaier, K. Günter, H. Moritz, and T. Esslinger, A Mott insulator of fermionic atoms in an optical lattice, *Nature* **455**, 204 (2008).
- [41] A. D. Ludlow, M. M. Boyd, J. Ye, E. Peik, and P. O. Schmidt, Optical atomic clocks, *Rev. Mod. Phys.* **87**, 637 (2015).
- [42] M. Mancini, G. Pagano, G. Cappellini, L. Livi, M. Rider, J. Catani, C. Sias, P. Zoller, M. Inguscio, M. Dalmonte, and L. Fallani, Observation of chiral edge states with neutral fermions in synthetic Hall ribbons, *Science* **349**, 1510 (2015).
- [43] A. J. Daley, M. M. Boyd, J. Ye, and P. Zoller, Quantum Computing with Alkaline-Earth-Metal Atoms, *Phys. Rev. Lett.* **101**, 1 (2008).
- [44] S. Ma, A. P. Burgers, G. Liu, J. Wilson, B. Zhang, and J. D. Thompson, Universal gate operations on nuclear spin qubits in an optical tweezer array of ^{171}Yb atoms, *ArXiv:2112.06799*.
- [45] K. Barnes, P. Battaglino, B. J. Bloom, K. Cassella, R. Coxe, N. Crisosto, J. P. King, S. S. Kondov, K. Kotru, S. C. Larsen, J. Lauigan, B. J. Lester, M. McDonald, E. Megidish, S. Narayanaswami, C. Nishiguchi, R. Notermans, L. S. Peng, A. Ryou, T.-Y. Wu, and M. Yarwood, Assembly and coherent control of a register of nuclear spin qubits, *Nat. Commun.* **13**, 2779 (2022).
- [46] J. Zeiher, Realization of Rydberg-dressed quantum magnets, PhD Thesis (2017), <https://doi.org/10.5282/edoc.21632>.